buildings

MDPI

Article

On the Shear Force Redistribution in Composite Steel and Concrete Beams with Web Openings

Jakub Bartus * and Jaroslav Odrobinak

Department of Structures and Bridges, Faculty of Civil Engineering, University of Zilina, Univerzitna 8215, 010 26 Zilina, Slovakia; jaroslav.odrobinak@uniza.sk
* Correspondence: jakub.bartus@uniza.sk

Abstract: As far as research into the field of composite steel and concrete beams with web openings has shown, the initiation of a complex stress state due to the introduction of web openings is, unfortunately, inevitable. As a logical consequence, estimation of the resistance becomes complex as well. Aiming to provide a more convenient approach, especially for evaluation of the bending resistance to the Vierendeel effect with the presence of high shear forces, a marked simplification with respect to quantification of the shear force redistribution between T-sections is presented. This novel approach stands on strong fundamentals of experimental evidence and parametric finite element (FE) investigation. Concretely, within the experimental part of this investigation, the load response of four composite beam samples was recorded and profoundly analyzed. Subsequently, a detailed FE analysis in the software ANSYS 2024 R1 (ANSYS Inc., Canonsburg, PA, USA), exploiting its parametric design language (APDL), was conducted. Finally, concise data compilation and their comprehensible interpretation were enabled by employing the software MATLAB 2024a (The MathWorks, Inc., Natick, MA, USA). In view of this treatment, a cornerstone for successive assessment of the obtained data was laid. Attempting to identify the key factors influencing the shear force proportion between the tees, integration of the shear stresses along the vertical sections with regular spacing along the FE beam models was conducted. By virtue of this concept, not only the magnitudes of the shear forces for the tees were obtained but also the leading importance of the opening depth was demonstrated. Furthermore, a complete picture of the shear force behavior along the composite perforated beams was derived. On this basis, a novel method representing a simpler and more accurate form of estimation of the shear force proportion for T-sections was proposed.

Keywords: composite beam; web opening; T-section; shear force redistribution; the Vierendeel effect

Citation: Bartus, J.; Odrobinak, J. On the Shear Force Redistribution in Composite Steel and Concrete Beams with Web Openings. *Buildings* **2024**, *14*, 1658. https://doi.org/10.3390/buildings14061658

Academic Editor: Hiroshi Tagawa

Received: 24 April 2024
Revised: 25 May 2024
Accepted: 28 May 2024
Published: 4 June 2024

1. Introduction

Composite structures are in general considered a highly efficient structural solution. They provide economic benefits owing to their quite rapid erection process, overall low self-weight, and versatile internal layout. Thus, they represent effective load-bearing systems for modern commercial buildings.

The main representative of composite load-bearing members constitutes composite beams, with a solid concrete slab coupled using headed shear studs with a hot-rolled I-steel section. Each of the above-mentioned components has inherent characteristics making this structural solution undoubtedly unique and hence challenging to design. Fortunately, for the mentioned type of composite beam, the current design standards [1,2] provide a sufficiently accurate approach.

However, when one or multiple web openings are introduced (for instance, due to the passage of service ducts), resistance calculation becomes notably complicated. Despite this, unabated demand for wider implementation of these structural elements has been witnessed and has yielded an estimable number of studies covering a large domain of related structural issues. In relation to the scope of this research, a quite extensive assemblage of

research works published by Granade [3], Todd and Cooper [4], Clawson and Darwin [5], and Redwood [6] has set the cornerstone for the current state of resistance calculation. In fact, the latest unified design approach can be found in the work of Lawson [7]. Therefore, its content served as a fundamental reference for the design of the experimental samples within this investigation. Through further analysis, the findings condensed in [8,9] led to the employment of asymmetric I-steel sections and openings with rounded corners in the experimental samples. In addition, the ideas proclaimed in [10,11] have provided fertile ground for the proposed enhancement of the current design concept with respect to the shear force redistribution between the tees.

The published works are a continuation of the already cited research, but they present other unique data based on theoretical and experimental investigations [12–14]. Alternatively, they also analyze the influence of different types and shapes of the openings in the steel webs on the overall bending behavior of steel–concrete composite beams [15,16].

Nevertheless, before diving deeper into the entire course of the investigation and presenting the recently derived findings, the application of the current approach will be revised.

2. Current Approach to the Vierendeel Bending Resistance

Despite great effort regarding research into composite steel–concrete perforated beams, no standardized design approach has been established yet. So, when analyzing this type of bearing member, a combination of the European standards and knowledge based on up-to-date research should be used.

Moving directly to a description of the Vierendeel effect, it is vital to give it an exact definition first. In its simplest form, the Vierendeel effect can be defined as the transfer of shear forces over the length of a web opening. Consequently, both the vertical and horizontal shear act on the lever arm and cause concentration of the stresses, predominantly at the opening's corners. From a mechanical point of view, this stress state can be interpreted by virtue of a simple mechanism, where the top and bottom tees are expressed as simply supported beams loaded by end moments (Figure 1). If this applies, a rise in additional bending stresses is unavoidable. Thus, the formation of local plastic hinges at specific locations is impending.

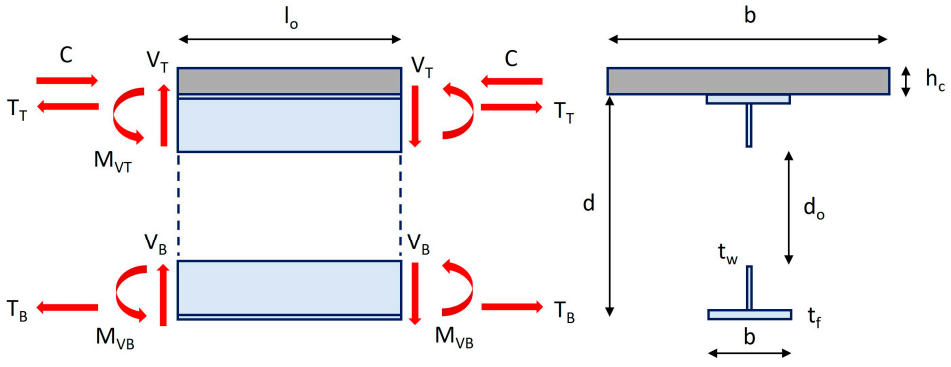

Figure 1. Mechanism of internal force transfer at the opening region.

Attempting to lessen these adverse effects, the opening shape, representing one of the most influencing factors, underwent serious investigation. A considerable number of research works have been published on this topic, where one of the most valuable [17] has unambiguously declared that curve-shaped web openings experience a lesser magnitude of local stresses. For this reason, the web openings introduced into the experimental samples had rounded corners.

Equally, as the shear resistance of a composite beam depends predominantly on the area of the steel web, with the presence of web openings, this resistance is significantly affected. As a result, the shear force bifurcates into the top and bottom tees of a beam.

A simplified portrayal of this phenomenon is illustrated using the shear force behavior along the composite samples (a) without and (b) with openings under the configuration of a four-point bending test (Figure 2). Concretely, the total shear force magnitude (TOT) is decomposed and assigned to the tees (TT—top tee, BT—bottom tee).

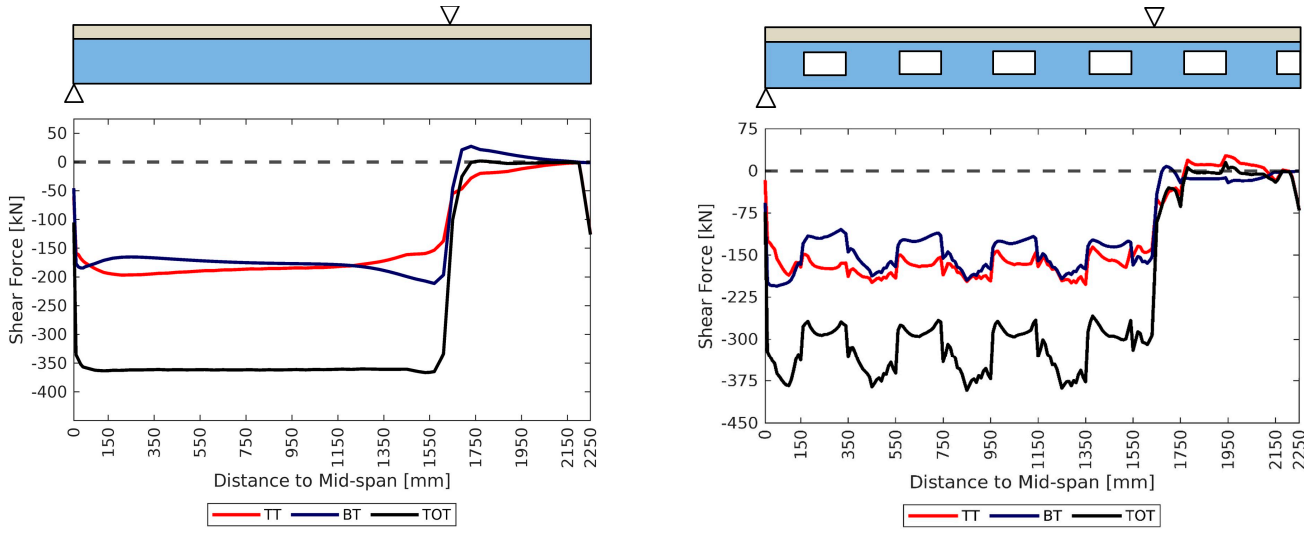

Figure 2. Shear force redistribution between the tees of a composite beam (**a**) without and (**b**) with web openings.

Indeed, this phenomenon plays a crucial role by estimation of the Vierendeel bending resistance at the opening centre, which is expressed as:

$$2 \cdot M_{tT,NV,Rd} + 2 \cdot M_{bT,NV,Rd} + M_{vc,Rd} \geq M_{vc,Ed}$$

where

$M_{tT,NV,Rd}$ = *the bending resistance of the bottom Tee, reduced for coexisting axial tension and shear*

$M_{bT,NV,Rd}$ = *the bending resistance of the top Tee, reduced for coexisting axial compression and shear*

$M_{vc,Rd}$ = *the local composite Vierendeel bending resistance*

$M_{vc,Ed}$ = $V_{Ed} . l_o$ *(the Vierendeel bending moment)*

where

V_{Ed} = *the design value of the vertical shear force*

l_o = *the effective length of an opening*

From the stated, it is clear, the resistance estimation can become quite indistinct when the coexistence of shear forces must be determined, especially if the redistribution of the shear forces is not clearly defined.

Attempting to solve this laborious task, a design approach adopting an iterative procedure was presented in [7]. A brief outline is as follows:

(1) The shear resistance of the bottom tee $V_{b,Rd}$ is first set to zero.
(2) The effective web thickness of the top tee $t_{w,eff}$ is evaluated.
(3) The plastic bending resistance of the top tee $M_{tT,NV,Rd}$ is determined.
(4) The plastic bending resistance for the bottom tee $M_{bT,NV,Rd}$ is estimated.
(5) The associated shear force in the bottom tee $V_{b,Ed}$ is evaluated as:

$$V_{b,Ed} = 2 \times M_{bT,NV,Rd} / l_o.$$

(6) The coexisting shear force in the top composite tee $V_{t,Ed}$ is figured as:

$$V_{t,Ed} = V_{Ed} - V_{b,Ed}.$$

(7) Then, the Vierendeel bending resistance is verified.
(8) If the verification does not meet these conditions, the utilization of the tees may be determined from the calculated values of $V_{t,Ed}$ and $V_{b,Ed}$, and the Vierendeel bending resistance is re-evaluated. A single iteration is generally adequate.

Even though the presented approach seems to be straightforward and easy to apply, it is not concise.

In addition, an even more simple approach exists [18], which basically attributes the shear resistance only to the top part of the composite section. The main prerequisite for this treatment is based on extensive utilization of the steel bottom tee in tension, thus reducing its carrying capacity for other actions.

The last alternative for the shear force redistribution concept [8] corresponds to a steel bottom tee with a proportion ranging from 10% to 40% of the total shear force.

Despite the existence of these basic concepts with regards to the shear force redistribution, the paucity of an exact definition impedes the way to a more accurate design procedure. Ergo, the core body of this research focuses on a detailed inspection of this subject, attempting to remedy the current state.

3. Applied Methodology

This research survey stands on three fundamental pillars—state-of-the-art analysis, experimental testing, and parametric FE investigation.

As is known, the first one represents a cornerstone for any investigation and has already been reviewed in the previous sections.

Turning to the second one, the experimental program conducted within this work is embodied by measurements of the deflection, slip, and deformation under the conditions of a four-point bending test. In total, four composite beam samples with a span of 4.5 m were tested. The load was introduced by controlled deformation. Twenty-two measurement gadgets were applied to every sample. Hence, quite a complex stress state could be recorded and subsequently analyzed.

Finally, an adequate FE investigation will be herein presented according to a comprehensive analysis carried out in the environment of the software ANSYS (2024 R1) APDL. To satisfy the strict requirements for the correlation between the experimental and numerical evidence, quite an extensive procedure was employed. In more detail, the following parts were included:

- Calibration of the input parameters for the Microplane constitution using an FE model of a cube.
- Estimation of properties for FE contact describing the shear connection.
- Creation of code exploiting looping processes for effortless changes in the input parameters for the FE model of the experimental samples.

Based on the mentioned approach, quite excellent compatibility between the data was attained.

4. Experimental Testing

Based on a mixture of evidence collected from standards [1,2], literature [7], and analytical–numerical studies [19,20] describing the behavior of perforated composite beams, the experimental survey was carried out.

4.1. Configuration of the Test Specimens

Attempting to meet the aims of this study, the configuration of the experimental specimens had to be designed in a way which allowed for considerable development of the Vierendeel effects and prevented the occurrence of other failure modes.

Focusing on the composite section, its steel part was designed using a fabricated asymmetric I-section. In general terms, this asymmetry is typically characterized as a ratio of the bottom to the top flange area ranging from 3 to 1. In our case, this ratio was at the level of 2.6. As a consequence, a sufficient resistance capacity in bending was guaranteed. The web openings were square in shape (200 × 200 mm) with rounded corners (a radius of 30 mm). They were centrically placed with respect to the web depth. This treatment ensured the avoidance of premature failure of the steel web due to the Vierendeel bending and allowed for the development of advanced strain magnitudes also for the other components of the composite beam. Moving onward, the solid parts of the steel web between openings, the web-posts, were of the same length as the openings, except for the end web-post. The concrete slab was designed as a solid with relevant reinforcement. A basic representation of the samples' configuration is illustrated in Figure 3.

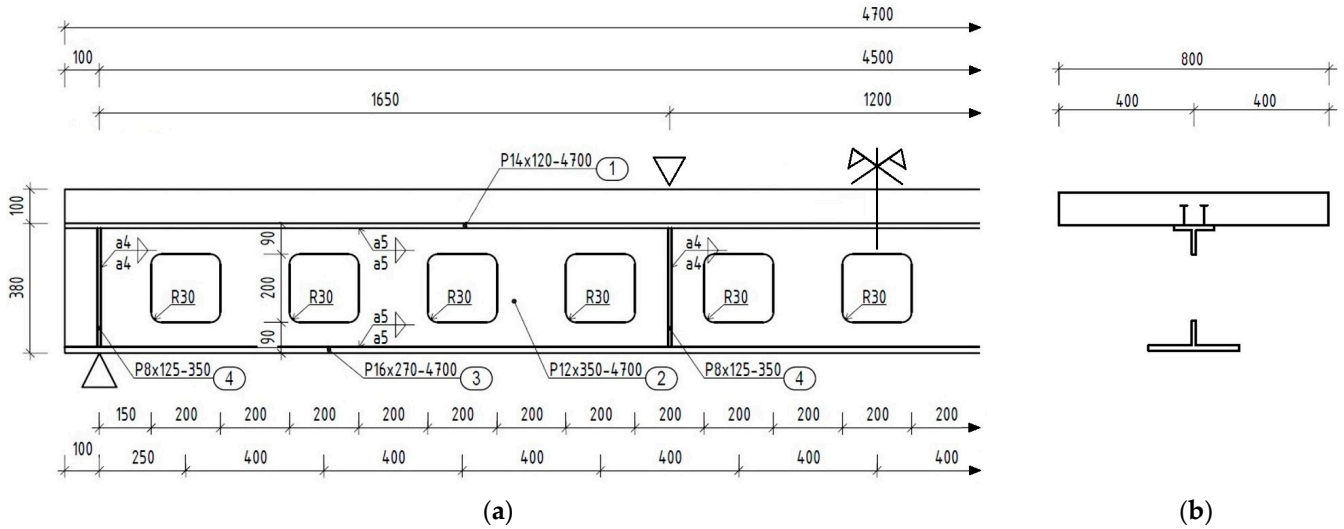

Figure 3. Side view (**a**) and cross-section (**b**) of the tested beam samples.

Additionally, the geometrical parameters of the investigated samples are summarized in Table 1.

Table 1. Overview of geometrical parameters of investigated samples.

Component	Width [mm]	Depth [mm]	Strength [MPa]	Detail of the Cross-Section
concrete slab	800	100	48	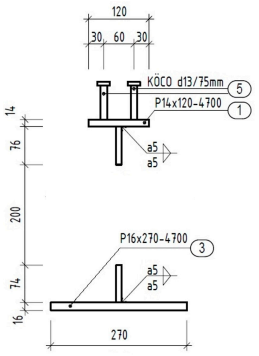
top flange	120	14	280	
web	12	350	276	
bottom flange	270	16	304	
opening	200	200	-	
shear stud	diameter [mm]	depth [mm]	strength [MPa]	
shank	13	67	327	
head	25	8		

Further, the connection at the steel–concrete interface was formed of two rows of headed shear studs. These connectors were designed to withstand not only the horizontal shear but also the tension loading initiated by the Vierendeel effect. In addition, on the basis of the arguments demonstrated in [19–21], partial attention has been devoted to investigation of the importance of the shear connection with respect to the overall load response.

In this case, a change in the shear connectors' layout was examined under two alternatives and presented the only variable parameter within the experimental measurements. In these, two beam samples were provided for each alternative from the total amount of four. The first alternative employed a uniform (BRU) distribution of studs, while the second one used non-uniform (BRN) spacing (Figure 4). For the latter alternative, the connectors were omitted above the openings but retaining the same number of shear connectors as with the BRU samples. Unfortunately, as will be shown later, this adjustment produced only negligible changes with respect to the overall load response documented according to the load–deformation and load–slip relations.

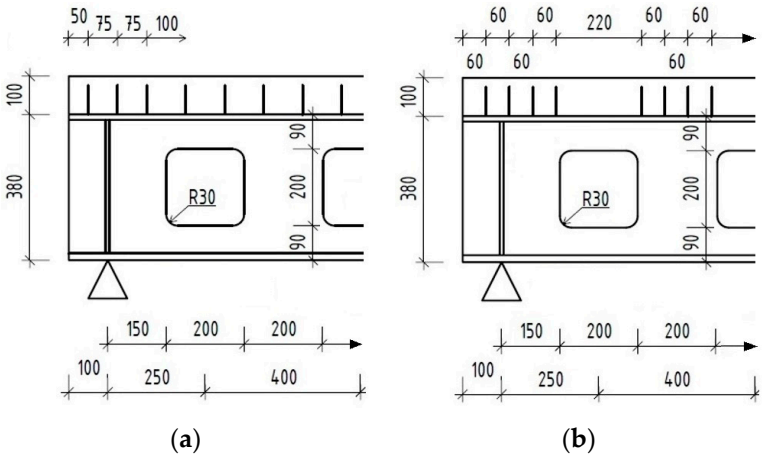

Figure 4. Alternative shear connector layouts using (**a**) uniform spacing (BRU) and (**b**) non-uniform spacing (BRN).

It must be added the overall configuration of beam samples was greatly affected by the set of design rules given in [7], which constitute not only the material aspects, loading conditions, and shear connections but specify size limits for the individual beam components as well.

Further, the configuration of the four-point bending test (Figure 5) was determined as the most appropriate since it provides a vital combination of actions—bending by high shear forces.

Figure 5. Illustration of the test set-up.

Through usage of this loading scheme, the possible occurrence of extreme stressing above the supports under the applied force must be considered. Therefore, web stiffeners were located at these critical positions. Additionally, a load spreader with elastic fillet have been installed between the hydraulic jack and the concrete slab to avoid excessive local stresses.

Ultimately, the correctness of the configuration of the experimental samples was approved by the preliminary FE analysis, which yielded the Vierendeel bending as the

major failure mode. This state can be clearly seen in Figure 6, where the formation of areas experiencing high-magnitude strains near the opening corners (red circles) could be observed in the preliminary FE model (Figure 6a) and in the real samples (Figure 6b). The latter was obtained as a consequence of the exhibition of the experimental samples to the exterior conditions represented by gradual corrosion, of course, after the loading process.

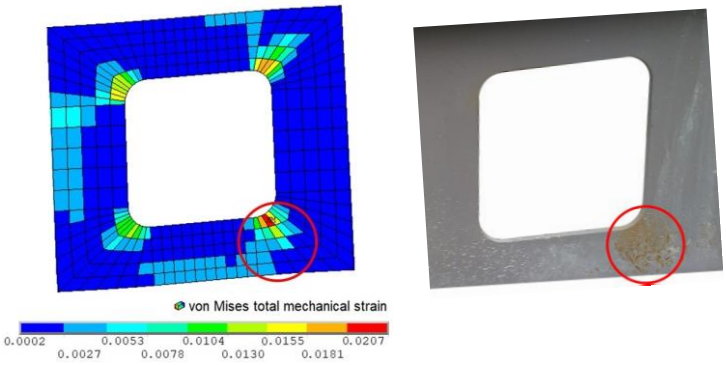

Figure 6. Failure mechanism representing the Vierendeel bending in the steel web from (**a**) the preliminary FE analysis and (**b**) an experimental sample.

4.2. Measurement Devices

Within this experimental program, a set of linear variable differential transducers (LVDTs) was used for displacement recording. In our experimental program, their main function was to capture the vertical deflection and slip. While the vertical deflection was measured at two positions, at the midspan (D1) and under the applied force (D2), the measurement of slip was recorded at the material interface using a unit of distance along the specimens (P1 to P5); see Figure 7.

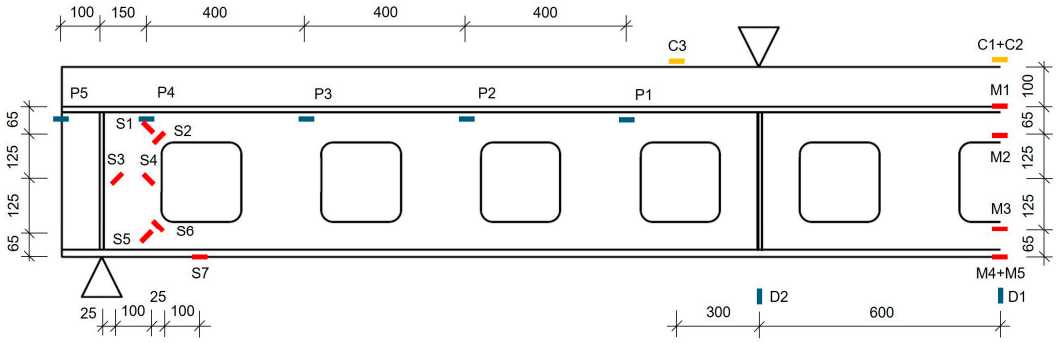

Figure 7. Configuration of the measurement gadgets.

Speaking of strain gauges measuring deformation, their positions were cautiously determined using the record and control principle. That meant a certain number of devices (C1 to C3, M1 to M5, S2, S3, S4, S6, S7) just recorded and stored the data to facilitate the picture of the overall stress state during the loading, while the others (S1, S5), having the control function, not only measured but also controlled the entire process of loading. To explain this in more detail, these gauges were applied at locations where the occurrence of the desired failure (the Vierendeel bending), represented by yielding due to extreme shearing, was expected.

In this way, the configuration of the measuring devices can be envisaged according to Table 2.

Table 2. Assignment of record and control principle to individual components.

Principle	**Beam Component**				
-	concrete slab	mat. interface	top flange	web	bottom flange
record	C1 to C3	P1 to P5	M1	M2 to M3 S2, S3, S4, S6	M4, M5, S7
control	-	-	-	S1, S5	-

To summarize the entire concept of the measurement device configuration, a simplified arrangement of both the LVDTs and the strain gauges is depicted in Figure 7.

It should be added that all the measured quantities were simultaneously recorded throughout the entire loading process, aiming to obtain the most exact stress projection for the subsequent parametric FE-based analysis.

4.3. Experimental Procedure

After execution of the primary steps of the experimental survey (rig set-up, dialing, and strain gauge application), the load was introduced by controlled deformation using a low displacement gradient. After that, it was applied in a stepwise manner, which means the loading process was interrupted at certain load levels in order to consider the relaxation effects.

To be specific, the samples were loaded gradually using 50 kN increments up to the first occurrence of yielding. This critical point in the loading process was reached nearly at the level of 600 kN. At this phase, the web next to the outermost opening at the location of the left corners (S1, S5) experienced the very first yielding. In other words, the Vierendeel bending took place (Figure 6). Subsequently, the increments were reduced to 5 kN per load step. At a load nearing 637 kN, yielding of the bottom flange at the midspan (M4, M5) occurred as well. Through subsequent loading, the process of advanced yielding without any significant change was observed. Hence, the process of loading was determined as accomplished at a deflection of 32 mm with achievement of 7.5% strains at the critical spots (S1, S5) for the desired failure mode. Picturing the entire process of loading, the load–deflection relations from positions D1 and D2 without relaxation effects are presented in Figure 8.

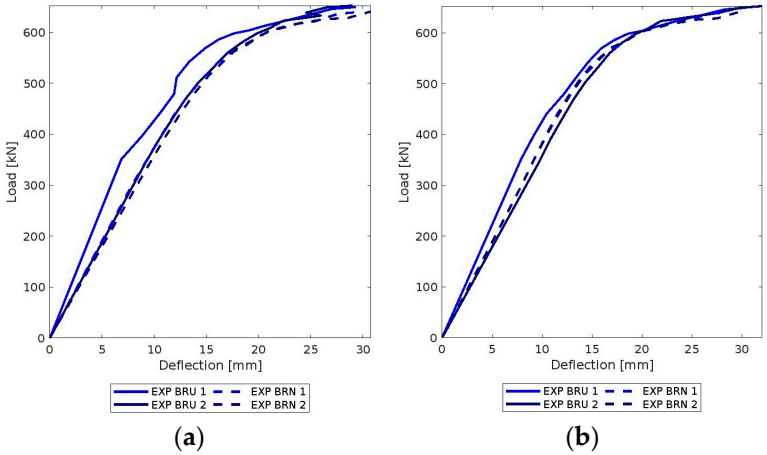

Figure 8. Load–deflection relations for the investigated specimens at positions (**a**) D1 and (**b**) D2.

Referring to the note from the previous section regarding the impact of the shear connectors' layout on the overall load response, no evident change was observed. On the contrary, there is a clear and significant agreement between the data recorded from individual experimental samples. A detailed discussion regarding the experimental data will be delivered in the following section concerning the validation of the reference FE model.

4.4. Material Properties

Examining the material properties of the steel part of the beam samples, a series of coupon tests were carried out in accordance with [22]. The samples were extracted from the unyielded regions of the composite beams at the level of web and the bottom flange. The mean values of the measured quantities can be found in Table 3.

Table 3. Mean values of measured quantities for the steel component of composite beam samples.

Beam Component	Depth [mm]	Width [mm]	Yield Strength [MPa]	Ultimate Strength [MPa]
web	12.00	13.65	276.16	423.49
bottom flange	15.83	13.40	304.00	424.51

The mixture for the concrete component of the investigated samples was made of a particular volume of water, a granular skeleton with a constant grain size, and a binding agent (commercially available cement without any particular properties). The samples used for the uniaxial compression test were cylindrical in shape with standardized dimensions. These samples were obtained in two fashions: by molding during concrete casting and core drilling after the execution of the test. The axial deformation measurements were carried out by a machine using deformation control. With the help of displacement sensors and software for data acquisition, the averaged axial deformations of the specimens were recorded. The limiting strength of concrete under compression reached the level of 46.18 MPa.

On these grounds, a set of reliable input parameters for the intended parametric FE investigation was established.

5. Reference Finite Element Model

In the following sections, a portrayal of the reference FE model, starting with the material perspective, going through a description of the elements, and ending with data correlation, will be delivered.

5.1. Concrete Component

Since the Microplane model seems to represent the material constitution most capable of properly capturing the inherent behavior of concrete under loading, its beneficial natures were fully exploited within this research content. Despite its significant competence, a slight complication related to the definition of its input parameters arises. So, as the Microplane model cannot be defined by typical stress–strain relations as with classical concrete constitutions, algorithmic code using the ANSYS parametric design language was developed. As a detailed description of this code would deserve an individual paper, only a brief outline follows:

- FE model of a cube $1 \times 1 \times 1$ mm in size is built.
- Meshing of the modeled cube with the element CPT215 is performed.
- Boundary conditions are applied.
- Changes in the load response under a combination of several parameters are examined according to an algorithmic process.

The material parameters are then verified by optimum fitting with respect to the fundamental stress–strain relations for concrete under uniaxial compression [23] and tension [24]. The correlation with the stress–strain relations is depicted in Figure 9, and an overview of the input parameters for the Microplane model is summarized in Table 4.

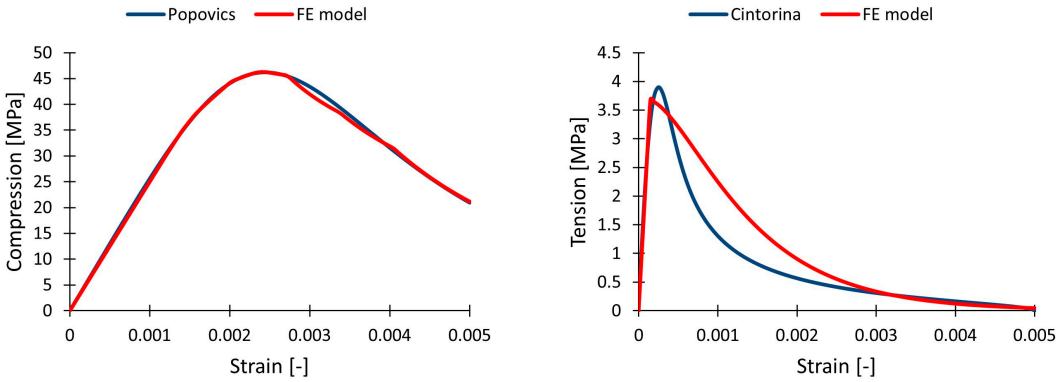

(**a**) (**b**)

Figure 9. Correlation of the numerical data with the stress–strain relations under (**a**) compression and (**b**) tension.

Table 4. Overview of input parameters for the Microplane model.

Material Parameters for Concrete	Label	Value
modulus of elasticity	e	31 GPa
Poisson's ratio	ν	0.18
uniaxial compressive strength	f_{uc}	46.18 MPa
biaxial compressive strength	f_{bc}	53.11 MPa
uniaxial tensile strength	f_{ut}	3.88 MPa
intersection between comp. cap and DP yield function	σ_{vc}	−35.41 MPa
ratio between the major and minor axes of DP cap	r	2
hardening material constant	d	80,000
tension cap hardening constant	r_t	1
tension damage threshold	γ_{t0}	0
compression damage threshold	γ_{c0}	1×10^{-4}
tension damage evolution constants	β_t	6000
compression damage evolution constants	β_c	2000
characteristic length of an element	l	50 mm
nonlocal interaction range parameter	c	4500 mm^2
over-nonlocal averaging parameter	m	2

The author would like to refer the reader, for a more detailed description of the mentioned parameters, to [25].

5.2. Steel Component

For the sake of preciseness, an accurate description of the stress–strain behavior for the steel elements in the FE model was of paramount importance. Ergo, constitutive equations [26] describing almost the full engineering stress–strain response of steel were employed. Even though this constitution is predominantly designated for hot-rolled carbon steels, it was applied in the FE models for a welded steel section that did not display any notable disparities. A simplified depiction of the applied stress–strain character with subsequent comparison to the experimental data is illustrated in Figure 10.

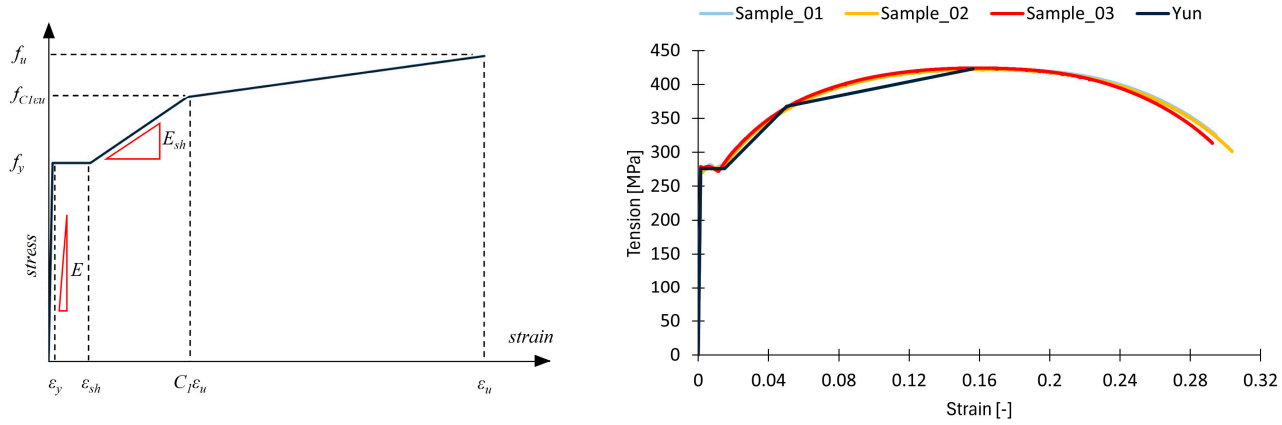

(**a**) (**b**)

Figure 10. Depiction of the applied stress–strain law for steel (**a**) with comparison to the experimental data (**b**).

5.3. Shear Connection

Commonly, as the simplest description of a shear connection in FE models of composite beams, a spring element is used [27]. On the one side, this alternative offers easy application; on the other side, it can lead to serious underestimation of the axial capabilities of connectors and the concentration of unrealistically large strains in the area of application.

Seeking more appropriate FE discretization, a 3D model of a shear stud seems to be apt. In this way, a shear stud is modeled as a volume object, commonly meshed with higher-order elements [28]. Then, the contact between the elements forming the shear studs and the surrounding concrete must be somehow defined. Hence, a set of different variables, for instance, normal stiffness, tangential stiffness, the general characteristics of the underlying materials and their constitutive descriptions, etc., have great potential to significantly affect or even limit the structural performance of this shear connection alternative. Respecting said, this method appears to be quite challenging.

As the last alternative for shear connection discretization (Figure 11), a 2D model working on the principles of surface-to-surface contact will be addressed. Particularly, this model represents the golden mean of the previously discussed alternatives. It exploits the spring model's simplicity and preserves partially the 3D model's complexity. Thus, the formation of a typical bearing cone is somewhat warranted.

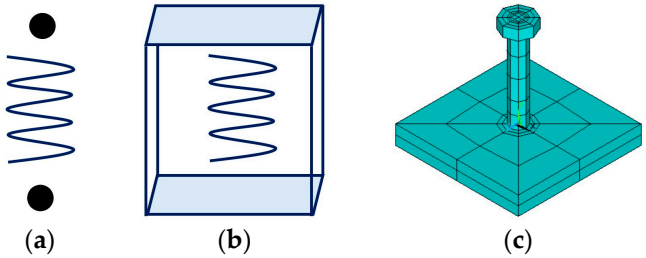

(**a**) (**b**) (**c**)

Figure 11. Alternatives for shear connection discretization in FE models: (**a**) 1D spring element, (**b**) 2D contact, (**c**) 3D model of shear stud.

Basically, as the Hertz theory [29] represents the bedrock of contact problem analysis, contact surfaces deform on the principles of elastic half-spaces. If one of the contacting bodies is significantly stiffer than the other, then the rigid-to-flexible contact accompanied by the unsymmetric (pair-based) option should be used in ANSYS. In this way, all the contact elements belong only to one specific surface, and all the target elements belong

to the other. On this basis, contact surface properties were assigned to the concrete slab, whereby the steel top flange was treated as the target surface [30].

As the next step, a particular type of contact regarding its structural response had to be defined. Considering the mechanical properties of headed shear studs, no-separation contact was selected as the most suitable type. Detailing the behavior of this contact, the typical load response of a shear connector was governed by suitable values of normal (FKN) and tangential (FKT) stiffness and the maximum frictional stress constraint (TAUMAX). It must be noted these characteristics were firstly evaluated for an individual shear connector and subsequently transformed into the two-dimensional domain by division of the sum of the individual shear connectors' resistance by the relevant area (Figure 12).

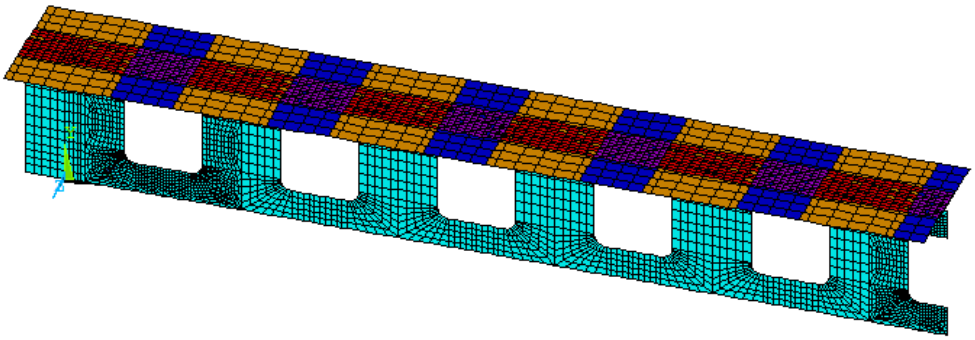

Figure 12. Illustration of area division at the material interface for application of uniform (BRU) and non-uniform (BRN) layouts of shear connectors.

To be specific, the axial stiffness of a shear connector was defined in accordance with [31] as:

$$k_{axial} = \frac{E_s \cdot A_s \cdot h_{ef}}{h_{ef}^2 + \frac{115}{10} \cdot n \cdot A_s} \quad (1)$$

where
E_s= *Young's modulus of steel used for a stud connector*
A_s= *cross − section area of a stud shank*
h_{ef}= *effective height of a shear stud embedment*
n = *ratio between* E_s/E_c, *where* E_c *is Young's modulus of concrete*

Further, the initial tangential stiffness was defined in reference to [18] using the formula:

$$k_{\tan} = \frac{D_{\max}}{d_{sh} \cdot (16/100 - 17/10000 \cdot f_c)} \quad (2)$$

where
D_{max}= *strength of a shear stud*
d_{sh} = *diameter of a stud shank*
f_c = *concrete strength in compression*

Finally, aiming to incorporate the typical plateau part of the force–slip curve expressing the slip behavior of the shear connection, a criterion of the maximum friction stress (TAUMAX) was defined from an equation describing the characteristic shear connector resistance [1]:

$$P_{Rk} = (8/10) \cdot f_u \cdot \pi \cdot d^2/4 \quad (3)$$

where
f_u= *ultimate tensile strength of a shear stud*
d = *diameter of a stud shank*

As two alternative of shear connector layouts were applied (BRU, BRN) for the beam samples, the same framework had to somehow be included in the reference FE model. So,

through the employment of an FE contact, the body of the FE was divided into a certain number of contact areas at the material interface, aiming to convey both the uniform (BRU) and non-uniform (BRN) layouts of the connectors. Hence, domains having full or no interactions were specified; see Figure 12.

In this context, the contact areas with full interactions were defined as effective areas under individual groups of shear connectors, which represented the exact part of contact resisting longitudinal shearing. Contrarily, the contact areas where no shear connectors were applied displayed characteristics of no interaction. That means the contact had almost no tangential resistance, thus allowing almost instant sliding.

5.4. Structure of the Finite Element Model

For discretization of the real samples, a combination of one-, two-, and three-dimensional elements was used. As for the steel bottom flange and web, these were modeled using the 2D elements SHELL181. On the other side, the steel top flange was discretized using the 3D elements SOLID185. Moving onward, the concrete slab was meshed with the solid elements CPT215. Here, it is important to note this element implements coupled physics capabilities (plasticity and damage); moreover, it provides implicit structural gradient regularization using a nonlocal field, which is one of its major capabilities enabling the proper simulation of concrete's behavior without any convergence difficulties. This ability is constituted by degrees of freedom at each corner node incorporating nonlocal field values (GFV1, GFV2, GFV3). Further, the reinforcement was described using LINK180, having appropriate coupling with the nodes of the elements constituting the concrete component. Finally, the shear connection was defined via TARGE170 and CONTA174. A plane illustration of the reference FE model is depicted below (Figure 13).

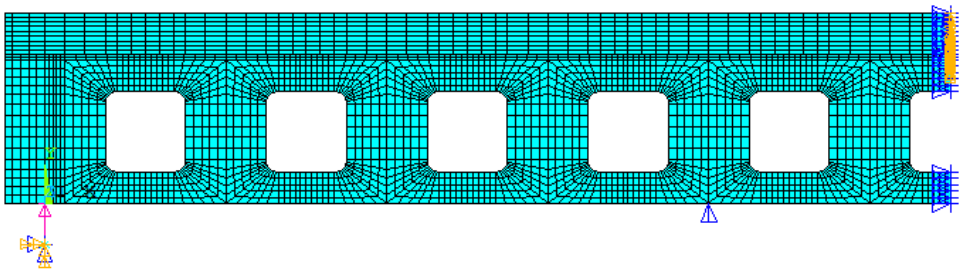

Figure 13. Reference finite element model.

5.5. Validation of the Finite Element Model

Publishing all the measured quantities would be extensive and potentially counterproductive, so only the most distinctive graphs corroborating the credibility of the reference FE model will be presented. These will show results detailing the load response with respect to different positions, materials, measured quantities, and magnitudes. The four experimentally tested specimens are blue in color, having solid lines (BRU) or dashed lines (BRN), while the reference FE models for both alternatives are red in color.

Firstly, load–deflection curves describing the overall behavior of the samples are shown in Figure 14. The presented data were measured at the positions labeled as D1 and D2. Although two alternatives for the shear connectors' layout were introduced, in all four tested beams, almost the same tendency in the load response could be observed. The maximum load, equal to 637 kN, was defined at a deflection of about 32 mm, which represents approximately 1/400 of the beams' span. Besides the quite excellent agreement, it could be noticed that the FE models behaved in a slight softer manner compared to the tested specimens. The main cause behind this lay in the maintenance of a safety margin.

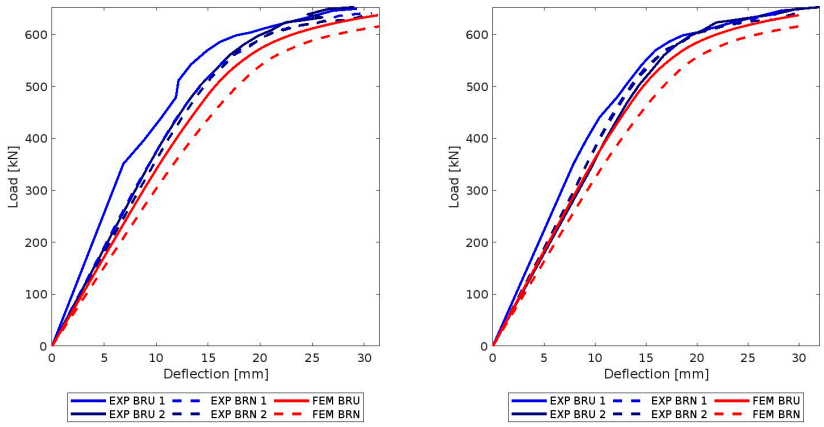

(**a**) (**b**)

Figure 14. Load–deflection relations at positions (**a**) D1 and (**b**) D2.

Secondly, deformations in the longitudinal direction were measured at the top level of the concrete slab (positions C1, C3). As a result of the application of the Microplane model within the FE model, negligible discrepancies were observed (Figure 15). Of note, these measurements were intended solely to complete the picture of the complex stress state occurring in the tested samples, so any significant observations were recorded. Since the concrete slab experienced contraction due to compression, the values use the negative sign. The same principle was applied to the steel elements.

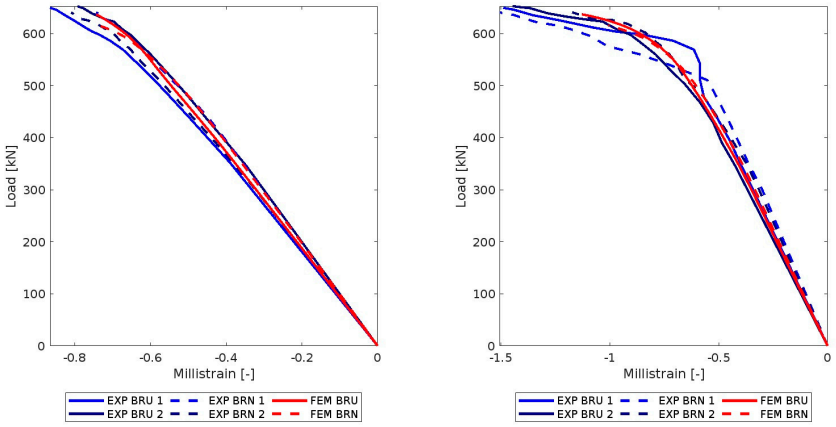

(**a**) (**b**)

Figure 15. Load–deformation relations at positions (**a**) C1 and (**b**) C3.

Thirdly, considering the steel part of the composite samples, the data recorded using the strain gauges applied at the center of the samples (M3, M4), within the pure bending zone, yielded the following results (Figure 16).

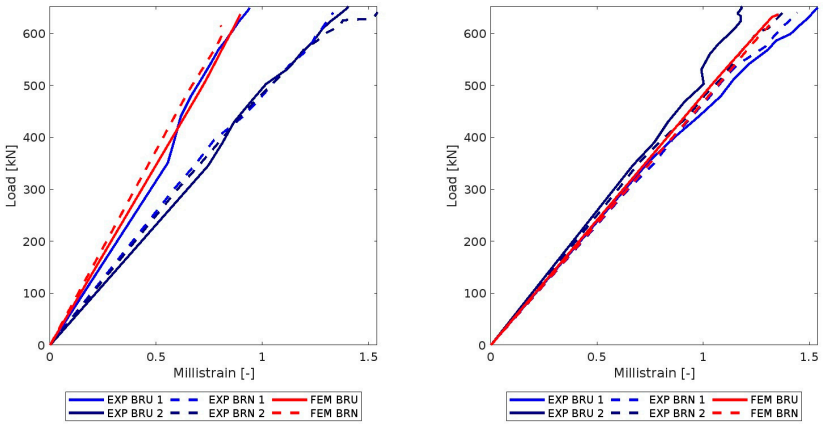

(**a**) (**b**)

Figure 16. Load-deformation relations at positions (**a**) M3 and (**b**) M4.

Concentrating on part (a) in Figure 16, the results unfortunately display small disparities. The reasoning for this adverse state might correspond to two perspectives. Firstly, exactly at this location in the FE models, symmetry constraints were applied. As a consequence, a slightly stiffer load response was produced in this region, so the deformations might be somewhat influenced. Secondly, as the 2D model of the shear connection, despite its capabilities, represents a quite significant simplification, it might produce to some extent inconsistent results. On the other side, these discrepancies were encountered only in this region, which implies the former suggestion could be correct, or this phenomenon was influenced by a partial combination of both factors. In addition, these measurements were taken in the vicinity of an opening edge (an area prone to yielding), so the exact deformation behavior is difficult not only to simulate but to record as well. Nevertheless, the outcomes from part (b) in Figure 16 coincide almost perfectly with the entire range of observed deformations.

Fourthly, the configuration of the foil gauges near the outermost web opening (S1, S5) was arranged in order to trace the principal strains. That means the gauges were placed under a 45-degree angle to the horizontal line. So, as the strains increased at these spots, significant magnitudes of strain were reported. These measurements are depicted below (Figure 17).

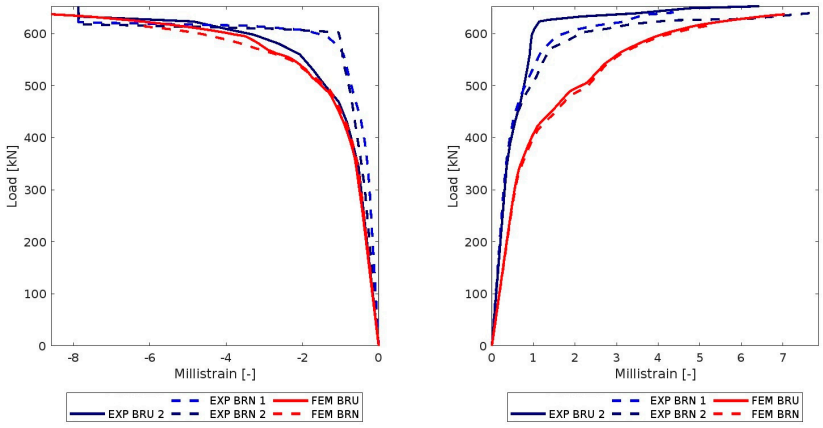

(**a**) (**b**)

Figure 17. Load–deformation relations at positions (**a**) S1 and (**b**) S5.

Accordingly, the Vierendeel bending mechanism causing yielding near the corners of the openings could be promptly distinguished. Interestingly, the rosettes documented almost an identical strain development, albeit with the employment of different shear connector layouts.

Finally, as the displacement at the material interface defines the slip behavior, these measurements helped us to identify changes in the overall load response because they quantified the development of slip strains. As Figure 18 documents, the non-uniform layout (BRN) led to a slightly softer response and larger values for slip in comparison to the uniform layout (BRU) at positions P2 and P3. The reasoning behind this phenomenon could lay in the different stressing of the shear connectors within the alternative layouts causing changes in the load response. Figuring this issue correctly, experimental measurements of the deformations directly at the shear studs would be needed.

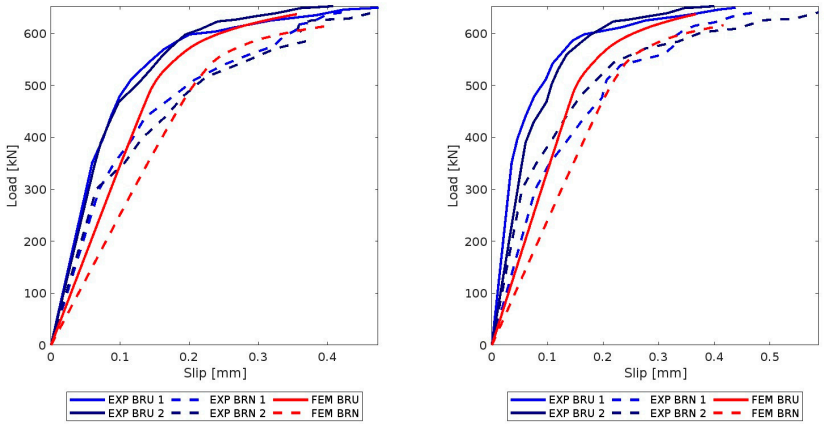

Figure 18. Load–slip relations at positions (**a**) P2 and (**b**) P3.

As can be seen, the overall stress state of the composite samples was quite precisely documented, and the observed discrepancies stayed in the acceptable range. On this basis, strong fundamentals for the credibility of the intended parametric FE investigation have been laid.

6. Parametric Finite Element Study

Before the presentation of any outcomes, it is a vital practice to describe the methodology behind their derivation. In order to interpret the distribution of the shear forces between the T-sections, the generation of vertical paths covering the individual depths of the tees and storing the variation in the shear stresses into a predefined matrix were carried out every 10 mm along the FE beam models. It must be explained that the borderline between the top and bottom tees was assumed to lay at the mid-depth of the steel web. Subsequently, integration corresponding to particular paths was conducted. In this way, the values of the shear forces with respect to the tees were derived. The results of this approach were already presented in Figure 2.

In addition, aiming to provide more explanatory outcomes, the shear force proportions were evaluated only at positions where the justification of the Vierendeel bending resistance is generally provided. Concretely, they were estimated at the centers of the web openings for calculation of the Vierendeel resistance exactly at these locations.

Trying to identify the key factor influencing the redistribution of the shear forces, an extensive parametric FE study was carried out. The following parameters were investigated:

- Concrete strength,
- Concrete slab depth,
- Steel strength,

- Bottom flange dimensions,
- Web dimensions,
- Opening dimensions.

Presenting the entire range of outcomes would be too excessive; therefore, findings regarding the mentioned parameters are given in Table 5. In this, the variation in specific parameters for individual samples and the change in the maximum values of the shear force proportion for the bottom tee compared to the reference sample are presented.

Table 5. Nature of variable parameters withing the parametric FE analysis.

	Parameter Value			Change	
Parameter Name	**Sample 1**	**Reference**	**Sample 2**	**Sample 1**	**Sample 2**
concrete strength	30 MPa	46.18 MPa	50 MPa	+1.1%	−0.1%
concrete slab depth	80 mm	100 mm	120 mm	+10.7%	−1.8%
steel strength	−10%	Table 3	+10%	−3.8%	+2.8%
bottom flange width	250 mm	270 mm	290 mm	−1.1%	+0.5%
web thickness	10 mm	12 mm	14 mm	−8.6%	+7.9%
webdepth	315 mm	350 mm	385 mm	−1.1%	+0.9%
opening length	100 mm	200 mm	300 mm	+7.3%	−7.7%
opening depth	100 mm	200 mm	300 mm	+16.2%	−54.5%

As can be seen, the opening's depth was found to play a major role in the redistribution of the shear forces between the T-sections. A detailed examination of this parameter, in relation to the opening size, is given in Table 6.

Table 6. Geometrical nature regarding variation in the opening depth.

Sample	**BT_100**	**BT_RF**	**BT_300**
opening length l_o	200	200	200
opening depth h_o	100	200	300
ratio l_o/h_o	2.00	1.00	0.67

Results capturing the influence of the adopted adjustment are illustrated below (Figure 19). In part (a) in the figure, the percentual proportion of the total shear force assigned to the bottom tee can be seen. The values for sample BT_100 range from 45.3% to 53.1%. On the other side, the values for sample BT_300 reflect a proportion spanning from 18.4% to 21.9%. This change is more evident in part (b) of Figure 19, wherein it is expressed as a ratio to the value for the reference sample BT_RF, which represents the FE model of the tested beams.

Concretely, sample BT_100 experienced an increase hovering at 16.2%, while sample BT_300 underwent a noteworthy decrease of up to 54.5%.

Based on these results, additional FE calculations were conducted. This treatment governed the change in the absolute depth of the web and opening by retaining their mutual relative depth ratios. In addition, as the beam span was also not modified, the findings' applicability corresponds only to beams with a ratio of the steel web depth to the beam span ranging from 1/11 to 1/15. The geometrical details are given in Table 7 (dimensions in mm).

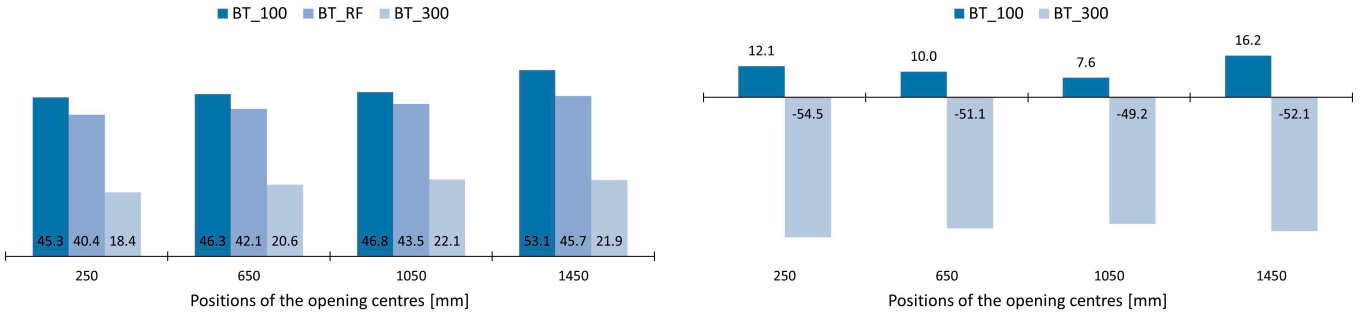

(**a**) (**b**)

Figure 19. Change in the shear force proportions for the bottom tee due to variation in the opening depth in (**a**) absolute and (**b**) ratio form.

Table 7. Geometrical characteristics covering additional FE calculations.

Ratio between Opening and Web Depth									
0.29		0.43		0.57		0.71		0.85	
Depth of									
Opening	**Web**	**Opening**	**Web**	**Opening**	**Web**	**Opening**	**Web**	**Opening**	**Web**
87	300	94	300	100	300	109	300	116	300
94	325	140	325	150	325	161	325	172	325
100	350	185	350	200	350	214	350	228	350
109	375	231	375	250	375	266	375	284	375
116	400	276	400	300	400	319	400	340	400

From the derived outcomes, only the maximum values for the shear force proportion from each specimen for either the top or bottom tee were taken, irrespective of the opening position. The reasoning behind this treatment laid in the provision of a certain resistance reserve.

Adopting the mentioned approach, two curves conveying the maximal values of the shear force proportions for the top (TT_max) and bottom (BT_max) tees under particular opening-to-web-depth ratios were established (Figure 20).

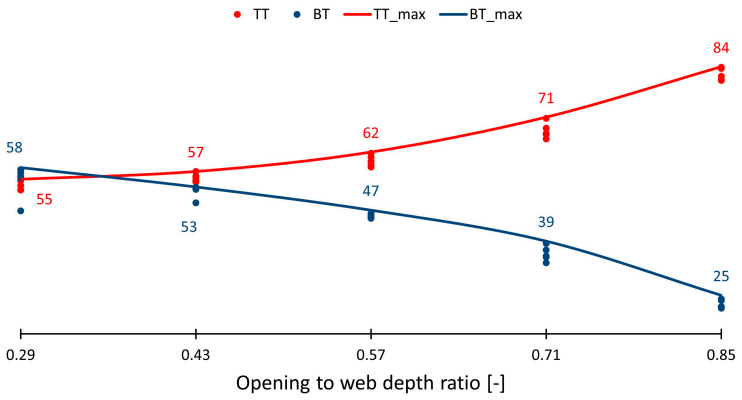

Figure 20. Redistribution of the shear force between the top and bottom tees.

As can be seen, the values of TT_max range from 55% to 84%, while the values of BT_max span from 25% to 58%.

On this basis, a novel concept defining the redistribution of the shear forces between the tees is proposed in the following section.

7. Novel Concept for Shear Force Redistribution between the Top and Bottom Tees in Composite Beams with Web Openings

Aiming to provide a more general form of the already presented findings, the relation defining the dependence of the shear force proportion for the Tees on the ratio between the opening and the web depth follows these equations:

$$top\ tee\ y = 0.55 + \frac{x^3}{2}; \tag{4}$$

$$bottom\ tee\ y = 0.65 - \frac{x^2}{2}; \tag{5}$$

$$function\ domain\ 0.29 \leq x \leq 0.85;$$

$$where$$
$$y = the\ shear\ force\ proportion$$
$$x = opening\ to\ web\ depth\ ratio$$

Focusing on the domain of functions (4) and (5), it is related to the configuration of the experimental samples and to the geometrical limits from [7]. These limits avert the transfer and subsequent development of severe plastic strains due to the Vierendeel bending at the level of the steel flanges.

A comparison of the results obtained from both the parametric FE analysis (TT_FEM, BT_FEM) and the newly derived relations ((4) TT_NC, (5) BT_NC) is graphically represented in Figure 21.

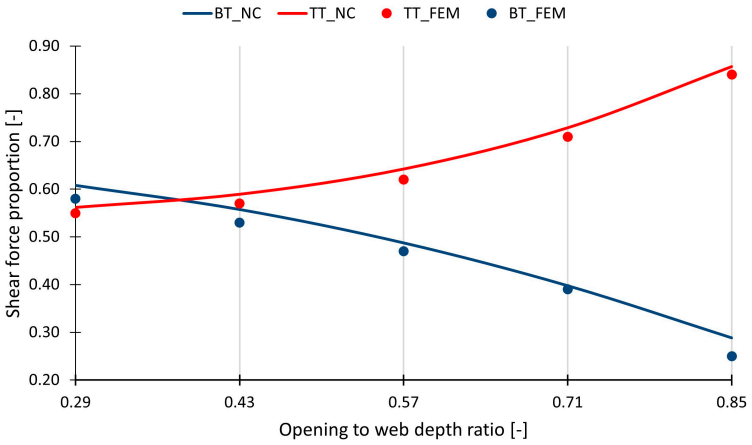

Figure 21. Proposed concept for definition of the shear force proportion for the tees.

Explaining this novel concept in detail, through the design of composite beams with web openings, as the ratio between the opening and the web depth is known (x-axis), the shear force assigned to the top tee $V_{t,Ed}$ is defined as multiplication of the design's shear force V_{Ed} by an appropriate shear force proportion (y-axis). The same principle applies for the bottom tee ($V_{b,Ed}$). The summation of $V_{t,Ed}$ and $V_{b,Ed}$ may produce values higher than the design shear force V_{Ed} due to the safety margin. Using this concept, the shear force redistribution is clear, and the condition stated in Section 6.2.8 in [2] on reduced moment resistance can be assessed for both tees.

8. Conclusions

Within this paper, two main objectives regarding composite beams with web openings underwent intense analysis:

(a) The impact of the shear connectors' layout.
(b) Shear force redistribution between the T-sections.

Attempting to derive credible outcomes, experimental testing followed by parametric FE investigation was conducted. The major outcomes of this investigation can be summarized as follows:

(a) The load response of composite beams with web openings reported a slightly softer response under a change from a uniform to a non-uniform layout of shear connectors. A similar outcome was documented for the slip behavior at the material interface. Different stressing of the individual connectors may be identified as the main cause behind this occurrence. To support this conclusion, detailed experimental investigation, for example, using deformation measurements directly at the connectors, would be needed. In conclusion, the impact of the layout of shear connectors on the overall load response was not as significant as expected.

(b) The opening depth was found to represent the key factor influencing the shear force redistribution between the tees of composite beams with web openings. According to the findings from the parametric FE analysis, the shear force proportions for the top tee lay between 55% and 84%, and for the bottom tee, they spanned from 25% to 58%.

(c) A novel concept defining the shear force redistribution between the tees was proposed. Compared to the current approach, it leaves out the iteration procedure and defines the shear force magnitudes using the opening-to-web-depth ratio. The procedure is applicable to beams with a ratio of web depth to beam span in the range of 1/11 to 1/15.

Despite the above demonstration, further validation of the proposed method on a broader scale of experimental samples is necessary. Hence, the authors believe the presented findings will stimulate further research activity aiming to verify what they have documented.

Author Contributions: Conceptualization, J.B.; supervision, J.O.; methodology, J.B.; experimental analysis, J.B. and J.O.; numerical validation, J.B.; parametric studies, J.B.; data analysis, J.B.; writing draft, J.B.; review and editing, J.O.; funding acquisition, J.O. All authors have read and agreed to the published version of the manuscript.

Funding: This research was supported by Research Project No. 1/0472/24 of the Slovak Scientific Grant Agency (VEGA).

Data Availability Statement: Raw data were generated at University of Zilina. Derived data supporting the findings of this study are available from the corresponding author J. Bartus on request.

Conflicts of Interest: The authors declare no conflicts of interest.

References

1. *EN 1994-1-1 (2004)*; Eurocode 4, Design of Composite Steel and Concrete Structures, Part 1-1: General Rules and Rules for Buildings. CEN: Brussels, Belgium, 2004.
2. *EN 1993-1-1 (2005)*; Eurocode 3, Design of Steel Structures, Part 1-1: General Rules for Buildings. CEN: Brussels, Belgium, 2005.
3. Charles, J.G. An Investigation of Composite Beams Having Large Rectangular Openings in Their Webs. Master's Thesis, University of Alabama at Tuscaloosa, Tuscaloosa, AL, USA, 1968.
4. Todd, D.M.; Cooper, P.B. Strength of composite beams with web openings. *J. Struct. Div.* **1980**, *106*, 431–444. [CrossRef]
5. Clawson, W.C.; Darwin, D. Strength of composite beams at web openings. *J. Struct. Div.* **1982**, *108*, 623–641. [CrossRef]
6. Redwood, R.; Cho, S.H. Design of steel and composite beams with web openings. *J. Constr. Steel Res.* **1993**, *25*, 23–41. [CrossRef]
7. Lawson, R.M.; Hicks, S.J. *Design of Composite Beams with Large Web Openings, SCI P355*; The Steel Construction Institute: London, UK, 2011.
8. Lawson, R.M.; Lim, J.; Hicks, S.J.; Simms, W.I. Design of composite asymmetric cellular beams and beams with large web openings. *J. Constr. Steel Res.* **2006**, *62*, 614–629. [CrossRef]
9. Chung, K.F.; Liu, C.H.; Ko, A.C.H. Steel beams with large web openings of various shapes and sizes: An empirical design method using a generalised moment-shear interaction curve. *J. Constr. Steel Res.* **2003**, *59*, 1177–1200. [CrossRef]
10. Classen, M. On the Structural Behavior of Composite Beams with Composite Dowels and Large Web Openings. Ph.D. Thesis, RWTH Aachen University Institute of Structural Concrete, Aachen, Germany, 2016.
11. Classen, M.; Kurz, W.; Schäfer, M.; Hegger, J. A mechanical design model for steel and concrete composite members with web openings. *Eng. Struct.* **2019**, *197*, 109417. [CrossRef]

12. Morkhade, S.G.; Gupta, L.M. Experimental investigation for failure analysis of steel beams with web openings. *Steel Compos. Struct.* **2017**, *23*, 647–656.
13. Lawson, R.M.; Hanus, F.; Sonck, D. Large web openings in steel and composite beams. *Steel Constr. Des. Res.* **2017**, *10*, 168–175. [CrossRef]
14. Ferreira, F.P.V.; Martins, C.H.; De Nardin, S. Advances in composite beams with web openings and composite cellular beams. *J. Constr. Steel Res.* **2020**, *17*, 106182. [CrossRef]
15. Liao, W.Y.; Zhou, D.H.; Li, L.Q. Analysis of composite beam with different web openings. *Adv. Constr. Technol.* **2014**, *919*, 15–18. [CrossRef]
16. Al-Rifaie, A.; Al-Husainy, A.S.; Al-Mansoori, T.; Shubbar, A. Flexural impact resistance of steel beams with rectangular web openings. *Case Stud. Constr. Mater.* **2021**, *14*, e00509. [CrossRef]
17. Tsavdaridis, K.D. Structural Performance of Perforated Steel Beams with Novel Web Openings and with Partial Concrete Encasement. Ph.D. Thesis, City University London, London, UK, 2010.
18. Oehlers, D.J.; Bradford, M.A. *Elementary Behaviour of Composite Steel and Concrete Structural Members*; Butterworth-Heinemann: Oxford, UK, 1999.
19. Bartus, J.; Odrobinak, J. Study on distribution of longitudinal shear forces in composite beams with web openings. *Transp. Res. Procedia* **2021**, *55*, 1221–1228. [CrossRef]
20. Bartus, J.; Odrobinak, J. Composite beams with web openings employing alternative layout of shear connectors. *Transp. Res. Procedia* **2023**, *74*, 1079–1086. [CrossRef]
21. Zeng, X.; Jiang, S.F.; Zhou, D. Effect of shear connector layout on the behavior of steel-concrete composite beams with interface slip. *Appl. Sci.* **2019**, *9*, 207. [CrossRef]
22. *EN ISO 6892-1:2019*; Metallic Materials—Tensile Testing—Part 1: Method of Test at Room Temperature. CEN: Brussels, Belgium, 2019.
23. Popovics, S.A. Numerical approach to the complete stress-strain curve of concrete. *Cem. Concr. Res.* **1973**, *3*, 583–599. [CrossRef]
24. Cintora, T. Softening Response of Concrete in Direct Tension. Master's Thesis, New Jersey Institute of Technology, Newark, NJ, USA, 1988.
25. Zreid, I.; Kaliske, M.A. Gradient enhanced plasticity–damage microplane model for concrete. *Comput. Mech.* **2018**, *62*, 1239–1257. [CrossRef]
26. Yun, X.; Gardner, L. Stress-strain curves for hot-rolled steels. *J. Constr. Steel Res.* **2017**, *133*, 36–46. [CrossRef]
27. Classen, M. Limitations on the use of partial shear connection in composite beams with steel T-sections and uniformly spaced rib shear connectors. *J. Constr. Steel Res.* **2019**, *142*, 99–112. [CrossRef]
28. Lam, D.; El-Lobody, E. Behavior of headed stud shear connectors in composite beam. *J. Struct. Eng.* **2005**, *131*, 96–107. [CrossRef]
29. Johnson, K.L. *Contact Mechanics*; Cambridge University Press: London, UK, 1985.
30. *Ansys® Academic Research Mechanical, Release 24.1, Help System, Structural Analysis Guide*; ANSYS, Inc.: Canonsburg, PA, USA, 2024.
31. Yang, F.; Liu, Y.; Liang, C. Analytical study on the tensile stiffness of headed stud connectors. *Adv. Struct. Eng.* **2019**, *22*, 1149–1160. [CrossRef]